IEICE TRANS. FUNDAMENTALS, VOL. E76-A, NO. 3 MARCH 1993

PAPER

Chaotic Phenomena in Nonlinear Circuits with Time-Varying Resistors

Yoshifumi NISHIO† *and* Shinsaku MORI†, *Members*

SUMMARY In this paper, four simple nonlinear circuits with time-varying resistors are analyzed. These circuits consist of only four elements; a inductor, a capacitor, a diode and a time-varying resistor and are a kind of parametric excitation circuits whose dissipation factors vary with time. In order to analyze chaotic phenomena observed from these circuits a degeneration technique is used, that is, diodes in the circuits are assumed to operate as ideal switches. Thereby the Poincaré maps are derived as one-dimensional maps and chaotic phenomena are well explained. Moreover, validity of the analyzing method is confirmed theoretically and experimentally.

key words: *chaos, parametric excitation circuit, one-dimensional map*

1. Introduction

Recently, studies on chaos are extensively carried out in a number of areas of natural science. In the area of electrical engineering, various chaos-generating circuits have been proposed and analyzed. Especially, in three-dimensional autonomous circuits or in two-dimensional nonautonomous circuits, the generation mechanism of chaos is being cleared theoretically.[1],[2]

On the other hand, parametric excitation circuits, namely a circuit with a element whose value varies with time, have studied in the area of nonlinear circuits. Especially, various nonlinear phenomena in some circuits whose natural frequency factor varies with time, have been investigated. In Refs. (3), (4), such circuits have been confirmed to generate chaos numerically. There are some systems whose dissipation factors vary with time, for example, under the time-variation of the ambient temperature, a equation describing a object moving in a space with some friction and a equation governing a circuit with a resistor whose temperature coefficient is sensitive such as thermistor. However, there are few discussions about chaotic phenomena is such systems.

In this paper, simple nonlinear circuits with time-varying resistors are analyzed. All these circuits consist of only four elements; a inductor, a capacitor, a diode and a time-varying resistor. These circuits are a kind of parametric excitation circuits whose dissipation factors varies with time and chaotic attractors are observed in three circuits. In order to analyze various chaotic phenomena in these circuits in detail, we use a degeneration technique, that is, we consider the case that the diodes in the circuits are assumed to operate as ideal switches. In this case, the Poincaré maps can be derived as one-dimensional maps and the generation of chaos and quasi-periodic attractors is well explained. This analyzing method have been proposed by Inaba et al.[5] and have been confirmed to be extremely effective to analyze some circuits including a diode.[6],[7] However, this method have not been applied for parametric excitation circuits. Lastly, the validity of the analyzing method is confirmed theoretically and experimentally.

2. Circuit Model

In this paper we concentrate our attention on the circuit family satisfying the following conditions.

1. The circuit consists of only four elements; a inductor, a capacitor, a diode, and a Time-Varying Resistor (TVR).
2. The circuit is governed by a two-dimensional nonlinear differential equation with time-varying coefficient.
3. Both of the diode and the TVR are connected in parallel with a capacitor or in series with a inductor.

The circuit family satisfying these conditions is one of the simplest models in the nonlinear systems whose dissipation factors vary with time. There are four circuits satisfying the above conditions and they are shown in Fig. 1. In the figures TVRs represent Time-Varying Resistors. The resistance $R_i(t)$ or the conductance $G_i(t)$ of TVRs varies with time. In this paper we consider the case that the function representing the variation of the TVRs is a square wave with angular frequency ω_{ti} and duty ratio p_i as shown in Fig. 2. Because in this case circuit experiments are extremely easy and we can analyze chaotic phenomena rigorously by using the general solution of the circuit equations. The advantages of the use of the general solution are follows. At first, we do not have to carry out numerical integrations on computer calculations. Secondly, we can show the validity of the idealization method of the diode theoretically. At last, we can derive the concrete representation of one-dimensional Poincaré maps obtained from the circuit models. The

Manuscript received April 2, 1992.

† The authors are with the Faculty of Science and Technology, Keio University, Yokohama-shi, 223 Japan.

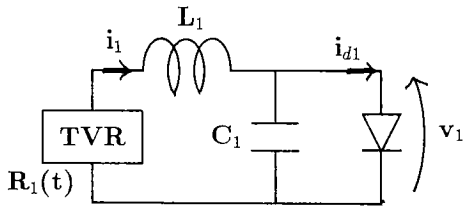

(a) Circuit 1.

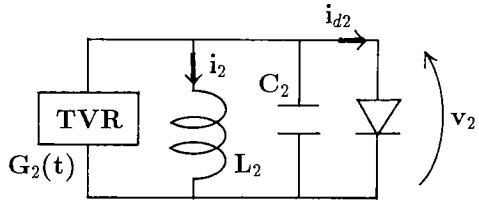

(b) Circuit 2.

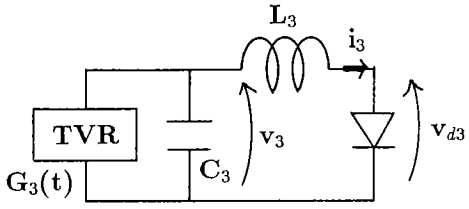

(c) Circuit 3.

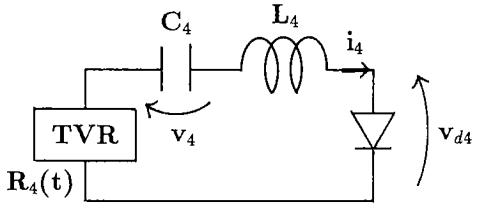

(d) Circuit 4.

Fig. 1 Circuit model (TVR is a Time-Varying Resistor).

case of a sinusoidal wave will be explained later.

At first, we approximate the $v-i$ characteristics of the diodes in the circuits by the following two-segment piecewise linear functions (see Fig. 3).

$$i_{di}(v_i)=\frac{G_{di}}{2}(v_i-V_i+|v_i-V_i|) \quad (i=1, 2)$$

$$v_{di}(i_i)=\frac{R_{di}}{2}\left(i_i+\frac{V_i}{R_{di}}-\left|i_i-\frac{V_i}{R_{di}}\right|\right) \quad (i=3, 4). \tag{1}$$

Then the circuit equations are given as follows

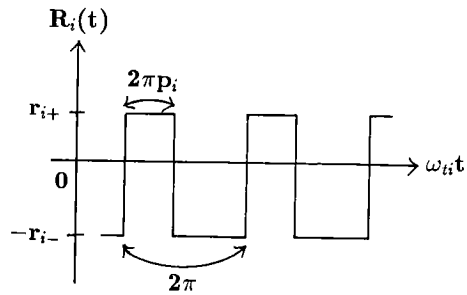

(a) i=1, 4.

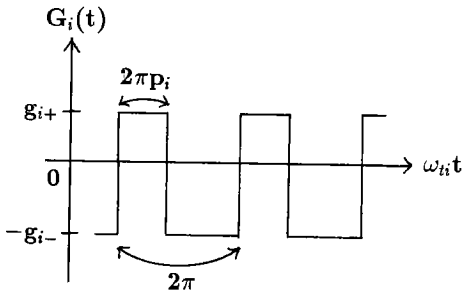

(b) i=2, 3.

Fig. 2 Characteristics of the TVRs.

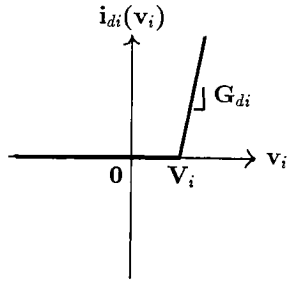

(a) i=1, 2.

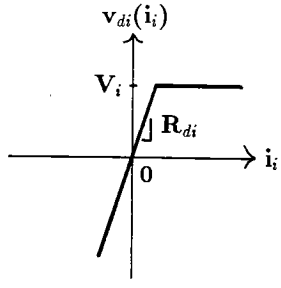

(b) i=3, 4.

Fig. 3 Characteristics of the diodes.

I. Circuit 1.

$$\begin{cases} C_1\dfrac{dv_1}{dt}=i_1-i_{d1}(v_1) \\ L_1\dfrac{di_1}{dt}=-v_1-i_1R_1(t) \end{cases} \tag{2}$$

II. Circuit 2.

$$\begin{cases} C_2\dfrac{dv_2}{dt}=-v_2G_2(t)-i_2-i_{d2}(v_2) \\ L_2\dfrac{di_2}{dt}=v_2 \end{cases} \tag{3}$$

III. Circuit 3.

$$\begin{cases} C_3\dfrac{dv_3}{dt}=-v_3G_3(t)-i_3 \\ L_3\dfrac{di_3}{dt}=v_3-v_{d3}(i_3) \end{cases} \tag{4}$$

IV. Circuit 4.

$$\begin{cases} C_4\dfrac{dv_4}{dt}=i_4 \\ L_4\dfrac{di_4}{dt}=-v_4-i_4R_4(t)-v_{d4}(i_4) \end{cases} \tag{5}$$

By changing the variables,

$$v_i=V_ix_i,\ i_i=\sqrt{\frac{C_i}{L_i}}V_iy_i,\quad t=\sqrt{L_iC_i}\,\tau,$$

$$\omega_{ti}=\frac{\omega_i}{\sqrt{L_iC_i}},$$

$$\text{“}\cdot\text{”}=\frac{d}{d\tau},\quad \frac{1}{\varepsilon_i}=\begin{cases} G_{di}\sqrt{\dfrac{L_i}{C_i}} & (i=1,\ 2) \\ R_{di}\sqrt{\dfrac{C_i}{L_i}} & (i=3,\ 4), \end{cases}$$

$$a_i=\begin{cases} r_i+\sqrt{\dfrac{C_i}{L_i}} & (i=1,\ 4) \\ g_i+\sqrt{\dfrac{L_i}{C_i}} & (i=2,\ 3) \end{cases},$$

$$b_i=\begin{cases} r_i-\sqrt{\dfrac{C_i}{L_i}} & (i=1,\ 4) \\ g_i-\sqrt{\dfrac{L_i}{C_i}} & (i=2,\ 3) \end{cases}. \tag{6}$$

the normalized circuit equations are given as follows.

I. Circuit 1.

$$\begin{cases} \dot{x}_1=y_1-D_1(x_1) \\ \dot{y}_1=-x_1-y_1f_1(\tau) \end{cases} \tag{7}$$

II. Circuit 2.

$$\begin{cases} \dot{x}_2=-x_2f_2(\tau)-y_2-D_2(x_2) \\ \dot{y}_2=x_2 \end{cases} \tag{8}$$

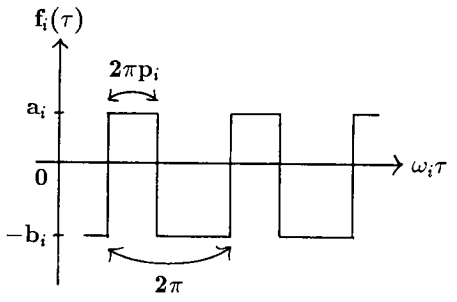

Fig. 4 $f_i(\tau)$ corresponding to $R_i(t)$ and $G_i(t)$.

III. Circuit 3.

$$\begin{cases} \dot{x}_3=-x_3f_3(\tau)-y_3 \\ \dot{y}_3=x_3-D_3(y_3) \end{cases} \tag{9}$$

IV. Circuit 4.

$$\begin{cases} \dot{x}_4=y_4 \\ \dot{y}_4=-x_4-y_4f_4(\tau)-D_4(y_4) \end{cases} \tag{10}$$

where $f_i(\tau)$ corresponds to the function switching the TVRs and is shown in Fig. 4. The function $D_i(\cdot)$ corresponds to the characteristics of the diodes and is represented as follows.

$$D_i(x_i)=\frac{1}{\varepsilon_i}\left(\frac{x_i-1+|x_i-1|}{2}\right)\quad (i=1,\ 2),$$

$$D_i(y_i)=\frac{1}{\varepsilon_i}\left(\frac{y_i+\varepsilon_i-|y_i-\varepsilon_i|}{2}\right)\quad (i=3,\ 4). \tag{11}$$

Define the following subspaces.

$$N_i\equiv\begin{cases} \{(x_i,\ y_i)\,|\,x_i<1\} & (i=1,\ 2) \\ \{(x_i,\ y_i)\,|\,y_i>\varepsilon_i\} & (i=3,\ 4), \end{cases}$$

$$M_i\equiv\begin{cases} \{(x_i,\ y_i)\,|\,x_i\geqq 1\} & (i=1,\ 2) \\ \{(x_i,\ y_i)\,|\,y_i\leqq\varepsilon_i\} & (i=3,\ 4). \end{cases} \tag{12}$$

Because Eqs. (7)-(10) are piecewise linear and $f_i(\tau)$ takes only two constant values, the general solutions can be given as follows.

• In the region N_i:

$$\begin{bmatrix} x_i(\tau) \\ y_i(\tau) \end{bmatrix}=\boldsymbol{F}_i(\tau)\cdot\boldsymbol{F}_i^{-1}(0)\cdot\begin{bmatrix} x_i(0) \\ y_i(0) \end{bmatrix}+\boldsymbol{P}_{Ni}(\tau) \tag{13}$$

where

$$\boldsymbol{F}_i(\tau)=\begin{bmatrix} \boldsymbol{f}_{xi}(\tau) \\ \boldsymbol{f}_{yi}(\tau) \end{bmatrix}. \tag{14}$$

In Eq. (14), $\boldsymbol{f}_{xi}(\tau)$ and $\boldsymbol{f}_{yi}(\tau)$ are given as follows.

$$\boldsymbol{f}_{xi}(\tau)=e^{\sigma_i(\tau)\tau}\begin{bmatrix} \cos\omega_i(\tau)\,\tau \\ \sin\omega_i(\tau)\,\tau \end{bmatrix}^T,\quad \boldsymbol{f}_{yi}(\tau)=\frac{d\boldsymbol{f}_{xi}(\tau)}{d\tau}$$

$$(i=1,\ 4) \tag{15}$$

$$\boldsymbol{f}_{yi}(\tau)=e^{\sigma_i(\tau)\tau}\begin{bmatrix}\cos\omega_i(\tau)\tau\\ \sin\omega_i(\tau)\tau\end{bmatrix}^T,\quad \boldsymbol{f}_{xi}(\tau)=\frac{d}{d\tau}\boldsymbol{f}_{xi}(\tau)\quad (i=2,\ 3)\quad (16)$$

where

$$\sigma_i(\tau)=-\frac{f_i(\tau)}{2},\quad \omega_i(\tau)=\frac{\sqrt{4-\{f_i(\tau)\}^2}}{2}\quad (17)$$

In Eq.(13), $\boldsymbol{P}_{Ni}(\tau)$ is given as follows.

$$\boldsymbol{P}_{N1}(\tau)=\boldsymbol{P}_{N2}(\tau)=\begin{bmatrix}0\\0\end{bmatrix},$$

$$\boldsymbol{P}_{N3}(\tau)=\begin{bmatrix}1\\-f_3(\tau)\end{bmatrix},\quad \boldsymbol{P}_{N4}(\tau)=\begin{bmatrix}-1\\0\end{bmatrix}.\quad (18)$$

• In the region M_i:

$$\begin{bmatrix}x_i(\tau)\\ y_i(\tau)\end{bmatrix}=\boldsymbol{G}_i(\tau)\cdot\boldsymbol{G}_i^{-1}(0)\cdot\begin{bmatrix}x_i(0)\\ y_i(0)\end{bmatrix}+\boldsymbol{P}_{Mi}(\tau)\quad (19)$$

where

$$\boldsymbol{G}_i(\tau)=\begin{bmatrix}\boldsymbol{g}_{xi}(\tau)\\ \boldsymbol{g}_{yi}(\tau)\end{bmatrix}.\quad (20)$$

In Eq.(20), $\boldsymbol{g}_{xi}(\tau)$ and $\boldsymbol{g}_{yi}(\tau)$ are given as follows.

$$\boldsymbol{g}_{x1}(\tau)=\begin{bmatrix}e^{\lambda_{1+}(\tau)\tau}\\ e^{\lambda_{1-}(\tau)\tau}\end{bmatrix}^T,\quad \boldsymbol{g}_{y1}(\tau)=\frac{d\boldsymbol{g}_{x1}(\tau)}{d\tau}+\frac{\boldsymbol{g}_{x1}(\tau)}{\varepsilon_1}\quad (21)$$

$$\boldsymbol{g}_{y2}(\tau)=\begin{bmatrix}e^{\lambda_{2+}(\tau)\tau}\\ e^{\lambda_{2-}(\tau)\tau}\end{bmatrix}^T,\quad \boldsymbol{g}_{x2}(\tau)=\frac{d\boldsymbol{g}_{y2}(\tau)}{d\tau}\quad (22)$$

$$\boldsymbol{g}_{y3}(\tau)=\begin{bmatrix}e^{\lambda_{3+}(\tau)\tau}\\ e^{\lambda_{3-}(\tau)\tau}\end{bmatrix}^T,\quad \boldsymbol{g}_{x3}(\tau)=\frac{d\boldsymbol{g}_{y3}(\tau)}{d\tau}+\frac{\boldsymbol{g}_{y3}(\tau)}{\varepsilon_3}\quad (23)$$

$$\boldsymbol{g}_{x4}(\tau)=\begin{bmatrix}e^{\lambda_{4+}(\tau)\tau}\\ e^{\lambda_{4-}(\tau)\tau}\end{bmatrix}^T,\quad \boldsymbol{g}_{y4}(\tau)=\frac{d\boldsymbol{g}_{x4}(\tau)}{d\tau}\quad (24)$$

where

$$\lambda_{i\pm}(\tau)=\begin{cases}\dfrac{-\{\varepsilon_i f_i(\tau)+1\}\pm\sqrt{\{\varepsilon_i f_i(\tau)+1\}^2-4\varepsilon_i\{\varepsilon_i+f_i(\tau)\}}}{2\varepsilon_i}\\ \quad (i=1,\ 3)\\ \dfrac{-\{\varepsilon_i f_i(\tau)+1\}\pm\sqrt{\{\varepsilon_i f_i(\tau)+1\}^2-4\varepsilon_i^2}}{2\varepsilon_i}\\ \quad (i=2,\ 4)\end{cases}\quad (25)$$

In Eq.(19), $\boldsymbol{P}_{Mi}(\tau)$ is given as follows.

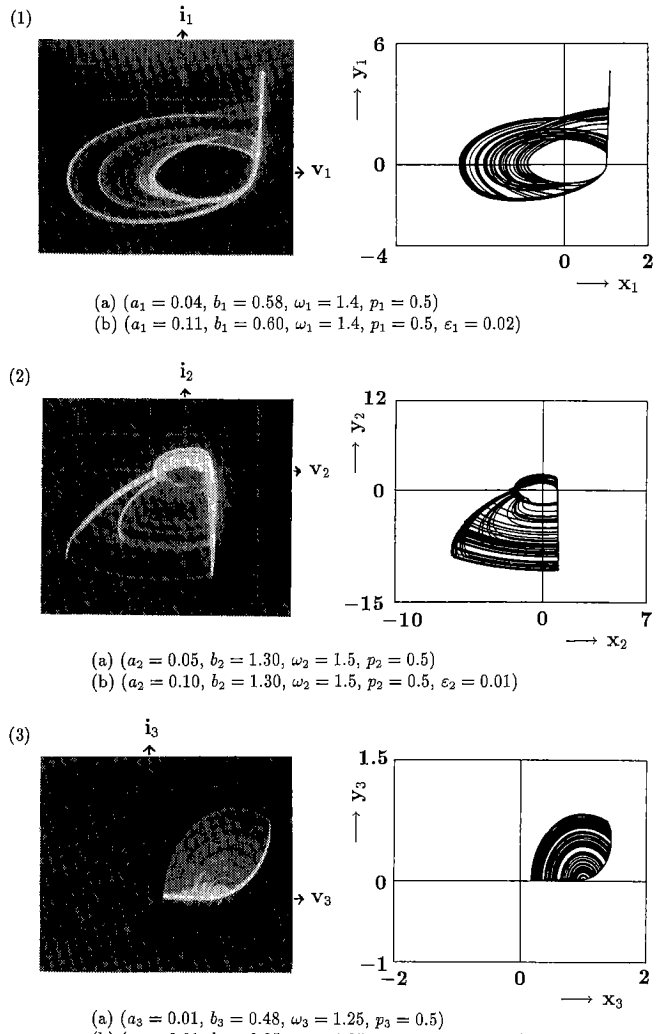

Fig. 5 Chaotic attractors obtained from
(1) Circuit 1, (2) Circuit 2, (3) Circuit 3.
(a) Experimental results.
(b) Computer calculated results.

$$\boldsymbol{P}_{M1}(\tau)=\begin{bmatrix}\dfrac{f_1(\tau)}{f_1(\tau)+\varepsilon_1}\\ -\dfrac{1}{f_1(\tau)+\varepsilon_1}\end{bmatrix},\quad \boldsymbol{P}_{M2}(\tau)=\begin{bmatrix}0\\ \dfrac{1}{\varepsilon_2}\end{bmatrix},$$

$$\boldsymbol{P}_{M3}(\tau)=\boldsymbol{P}_{M4}(\tau)=\begin{bmatrix}0\\0\end{bmatrix}\quad (26)$$

The experimental and computer calculated results are shown in Fig. 5. In the circuit experiments, the TVR is realized by using an analog switch shown in Fig. 6. We found chaotic attractors from the circuits 1 -3. In the circuit 4, we cannot found chaotic attractors and for any parameter values the solution converges to

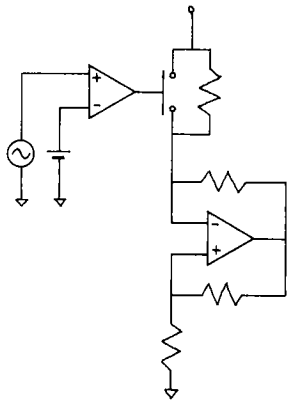

(a) Current controlled type (for Circuit 1 and 4).

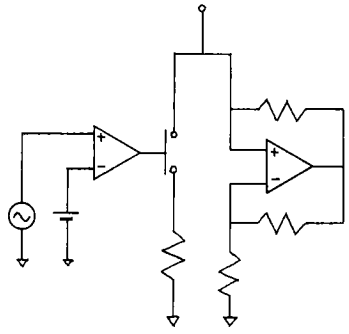

(b) Voltage controlled type (for Circuit 2 and 3).

Fig. 6 Circuit realization of the TVR.

the origin or diverges to infinity (the operational amplifier saturates in the circuit experiments). This reason will be explained as follows. Because the diode in the circuit 4 is connected in series with the TVR, the stability of the origin is decided by the sum of resistance of the diode when it is off-state and resistance of the TVR. Since the resistance of the diode when it is off-stage is relatively large, the negative resistance of the TVR is needed to be large value in order to generate the oscillation, that is, $R_{d4} < r_{4-}$. However, when the oscillation amplitude becomes larger and the diode turns on, the solution diverges immediately because the resistance of the diode when it is on-state is relatively small.

3. Idealization of Diodes

The analysis of continuous chaos is routinely done by the mapping method. In this case, the proof of the generation of chaos is extremely difficult due to insufficient mathematical discussions on the discrete dynamical system of more than two-dimension. Therefore, in the following, we analyze the circuits 1-3 by using a degeneration technique, that is, we consider the case that the diodes in the circuits are assumed to operate as ideal switches. The analysis of the model

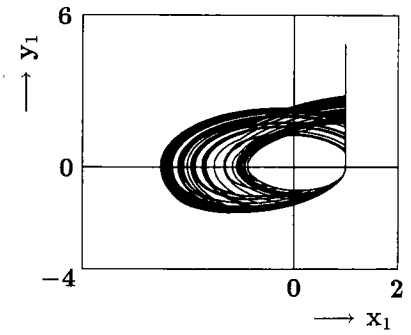

(a) ($a_1 = 0.11$, $b_1 = 0.60$, $\omega_1 = 1.4$, $p_1 = 0.5$)

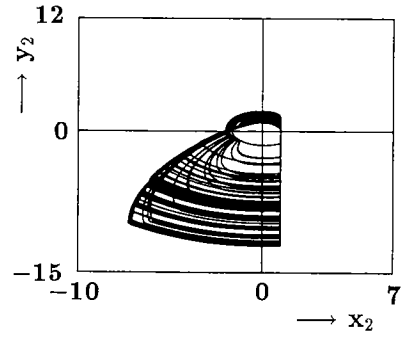

(b) ($a_2 = 0.10$, $b_2 = 1.35$, $\omega_2 = 1.5$, $p_2 = 0.5$)

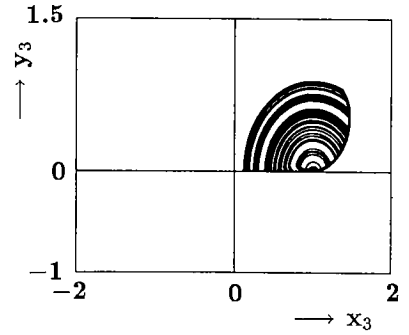

(c) ($a_3 = 0.01$, $b_3 = 0.35$, $\omega_3 = 1.25$, $p_3 = 0.5$)

Fig. 7 Chaotic attractors obtained from the circuit models with the idealized diodes.
(a) Circuit 1, (b) Circuit 2, (c) Circuit 3.

with such a degeneration is much simpler than the direct analysis of (7)-(9).

First, let us provide the idealization of diodes.

1. The diode takes either ON-state or OFF-state.
2. The diode at ON-state operates as a constant voltage source with voltage V_i and the diode at OFF-state operates as open.
3. The diode turns off when the current through it becomes zero and turns on when the voltage across it reaches V_i.
4. The voltage across the capacitor and the current through the inductor is continuous.

This idealization corresponds to the limit $(G_{di}, R_{di}) \rightarrow$

(∞, ∞) in Fig. 3.

In the case that the above idealization technique is used, the circuit equations in the regions M_i are degenerated as follows.

I. Circuit 1.

$$\begin{cases} (x_1=1) \\ \dot{y}_1=-1-y_1 f_1(\tau) \end{cases} \tag{27}$$

II. Circuit 2.

$$\begin{cases} (x_2=1) \\ \dot{y}_2=1 \end{cases} \tag{28}$$

III. Circuit 3.

$$\begin{cases} \dot{x}_3=-x_3 f_3(\tau) \\ (y_3=0) \end{cases} \tag{29}$$

The transitional conditions to the regions M_i from N_i are given as follows.

I. Circuit 1.

$$y_1=0 \tag{30}$$

II. Circuit 2.

$$y_2+f_2(\tau)=0 \tag{31}$$

III. Circuit 3.

$$x_3=1 \tag{32}$$

Here Eqs. (30), (31) represent that the currents through the diodes become zero and Eq. (32) represents that the voltage across the diode reaches the threshold voltage V. For instance, the currents through the diode in the ON-state in the circuit 1 can be obtained by letting $dv_1/dt=0$ in Eq.(2). Figure 7 shows examples of chaotic attractors obtained from the models with the idealized diodes.

4. Validity of Idealization of Diodes

In this section, validity of the idealization of diodes in the previous section is confirmed theoretically. Note that the derivation of the general solutions enables us to show the validity of the idealization.

At first, define the following eigenspaces corresponding the eigenvalues in Eq. (25).

$$\lambda_{i\pm}(\tau) \to E_{i\pm}(\tau) \quad (i=1, 2, 3) \tag{33}$$

In the case of $\varepsilon_i \to 0$, the following equations are satisfied.

$$\lim_{\varepsilon_i \to 0} \lambda_{i-}(\tau) = -\infty \quad (i=1, 2, 3). \tag{34}$$

$$\lim_{\varepsilon_i \to 0} E_{i+}(\tau) = \{(x_i, y_i) | x_i=1\} \quad (i=1, 2),$$

$$\lim_{\varepsilon_3 \to 0} E_{3+}(\tau) = \{(x_3, y_3) | y_3=0\}. \tag{35}$$

$$\lim_{\varepsilon_1 \to 0} \{E_{1+}(\tau) \cap (x_1=1)\} = \{(x_1, y_1) | y_1=0\},$$

$$\lim_{\varepsilon_2 \to 0} \{E_{2+}(\tau) \cap (x_2=1)\} = \{(x_2, y_2) | y_2+f_2(\tau)=0\},$$

$$\lim_{\varepsilon_3 \to 0} \{E_{3+}(\tau) \cap (y_3=\varepsilon_3)\} = \{(x_3, y_3) | x_3=1\}. \tag{36}$$

The proof of the above equations is provided in the Appendix.

The meaning of the above equations is as follows. For example, consider the solution entering the region M_1. In M_1 the eigenspace $E_{1+}(\tau)$ converges to $x_1=1$ and λ_{1-} indicating the degree at which the solution is constrained by $E_{1+}(\tau)$ is $-\infty$. Hence, this solution is constrained to the boundary surface $x_1=1$. Moreover, consider the case where this constrained solution is returned to N_1. Since the solution is constrained to $E_{1+}(\tau)$, it enters N_1 from the intersection of $E_{1+}(\tau)$ and $x_1=1$. This intersection converges to $y_1=0$, that is, the transitional condition of the idealized model (Eq. (30)). Therefore, the vector fields of the original differential equations (7)-(9) converge to the idealized model (27)-(32) and the motion of the solutions of our circuit models seems to be explained by the models with the idealized diodes.

5. Poincaré Map

In the case that the idealization method in the Sect. 3 is used, the circuit equations are degenerated piecewisely and one-dimensional Poincaré maps can be derived strictly.

At first, we explain the derivation of the Poincaré map corresponding to the circuit 1.

In the circuit 1, when the solution enters the region N_1 from M_1, namely when the diode turns off, $(x_1, y_1)=(1, 0)$ is satisfied. Hence, only the phase of the square wave switching the TVR decides the following motion of the solution.

We consider the solution starting from the point $(x_1, y_1)=(1, 0)$ at $\tau=0$. Let the phase of the function switching the TVR be $\phi_1(n)$ (see Fig. 8). The solution hits the boundary $x_1=1$ at some proper time $\tau=\tau_{1a}$ and enters the region M_1 from a point $(x_1, y_1)=(1, \hat{y}_1)$. This solution moves on the line $x_1=1$ and reaches $(x_1, y_1)=(1, 0)$ at some proper time $\tau=\tau_{1a}+\tau_{1b}$ under adequate parameter set.

The value of $\phi_1(n+1)$; the phase of the function

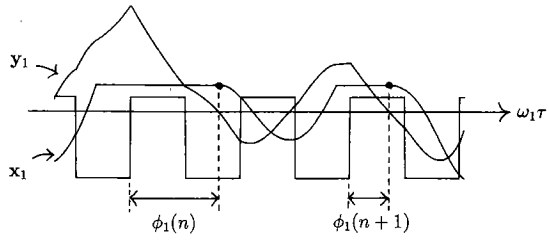

Fig. 8 Derivation of the Poincaré map.

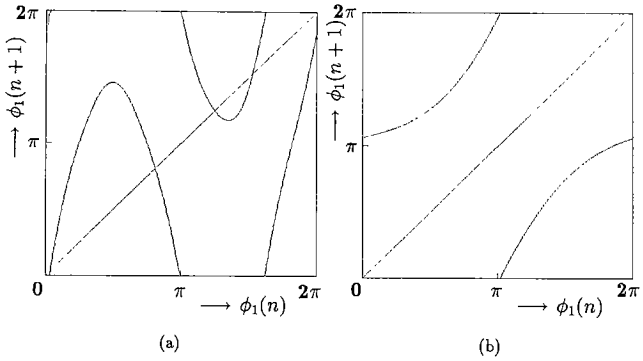

Fig. 9 Poincaré map T_1 (circuit 1).
(a_1=0.11, b_1=0.6, p_1=0.5).
(a) ω_1=2.0.
(b) ω_1=3.0.

switching the TVR when the solution returns back to the point (1, 0), is given as follows.

$$\phi_1(n+1)=\{\phi_1(n)+\omega_1(\tau_{1a}+\tau_{1b})\}\text{mod } 2\pi \quad (37)$$

τ_{1a} is given by calculating the following implicit equation

$$1=[1 \quad 0]\cdot\boldsymbol{F}_1(\tau_{1a})\cdot\boldsymbol{F}_1^{-1}(0)\cdot\begin{bmatrix}1\\0\end{bmatrix} \quad (38)$$

$\hat{y}_1$ is given as follows

$$\hat{y}_1=[0 \quad 1]\cdot\boldsymbol{F}_1(\tau_{1a})\cdot\boldsymbol{F}_1^{-1}(0)\cdot\begin{bmatrix}1\\0\end{bmatrix} \quad (39)$$

τ_{1b} is given by calculating the following implicit equation

$$\left\{\hat{y}_1+\frac{1}{f_1(0)}\right\}e^{-f_1(\tau_{1b})\tau_{1b}}-\frac{1}{f_1(\tau_{1b})}=0 \quad (40)$$

Then the Poincaré map T_1 can be derived as one-dimensional map which transforms the n-th phase $\phi_1(n)$ into the $(n+1)$-th phase $\phi_1(n+1)$. Figure 9 shows two examples of T_1 obtained by calculating (37)-(40). We confirmed that T_1 has the following feature by computer calculations. T_1 has discontinuity for $\omega_1<\omega_{1D}\cong 1$. T_1 is noninvertible for $\omega_{1D}<\omega_1<\omega_{1C}\cong 2.9$. T_1 is homeomorphic for $\omega_{1C}<\omega_1$. For $\omega_{1D}<\omega_1$ the form of T_1 is similar to the sine-circle map.[8],[9] The sine-circle map has been studied extensively and has been confirmed to generate chaotic and quasi-periodic attractors. Various chaotic phenomena observed from the circuit 1 are well explained by the sine-circle map. Namely, chaotic attractors can be generated for $\omega_{1D}<\omega_1<\omega_{1C}$ and quasi-periodic and periodic states appear and disappear alternately for $\omega_{1C}<\omega_1$. The 1-parameter bifurcation diagram of T_1 is shown in Fig. 10.

Next, in the circuit 2, the solution in the region M_2 must go through the point $(x, y)=(1, -a_2)$. Hence, when the solution is on the point $(1, -a_2)$, only the

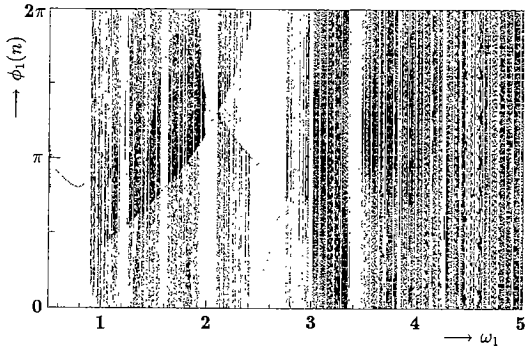

Fig. 10 1-parameter bifurcation diagram of T_1 (circuit 1).
(a_1=0.11, b_1=0.6, p_1=0.5).

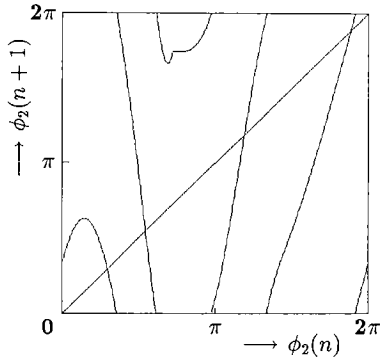

Fig. 11 Poincaré map T_2 (circuit 2).
(a_2=0.10, b_2=1.35, ω_2=1.2, p_2=0.5).

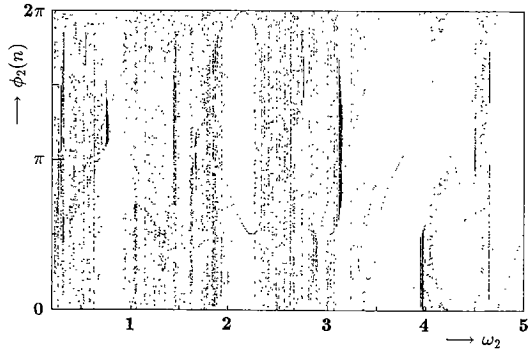

Fig. 12 1-parameter bifurcation diagram of T_2 (circuit 2).
(a_2=0.10, b_2=1.35, p_2=0.5)

phase of the square wave decides the following motion of the solution. Therefore, the Poincaré map T_2 can be derived as one-dimensional map as similar to the case of the circuit 1. Figure 11 shows an example of T_2. The derivative of T_2 has a discontinuity because there are two routes from the point $(1, -a_2)$ to the same point. Due to the existence of this discontinuity, the bifurcation phenomena are relatively complicated. The 1-parameter bifurcation diagram of T_2 is shown in Fig. 12.

At last, in the circuit 3, when the solution enters the region N_3 from M_3, namely when the diode turns

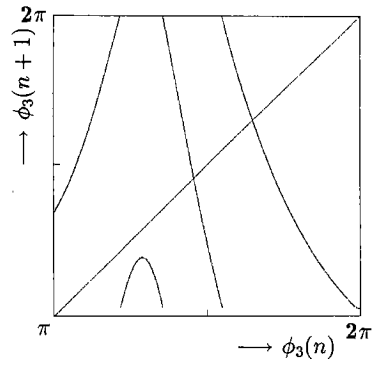

Fig. 13 Poincaré map T_3 (circuit 3).
(a_3=0.01, b_3=0.35, ω_3=0.7, p_3=0.5)

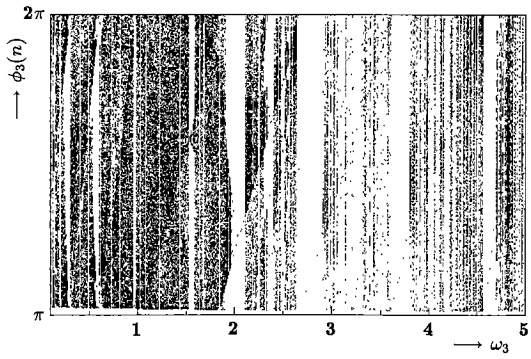

Fig. 14 1-parameter bifurcation diagram of T_3 (circuit 3).
(a_3=0.01, b_3=0.35, p_3=0.5)

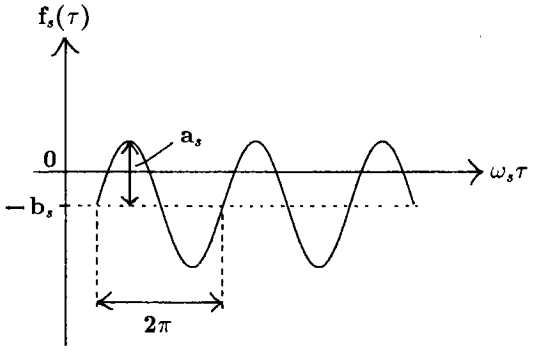

Fig. 15 Characteristics of the TVR varying sinusoidally.

on, $(x_3, y_3) = (1, 0)$ is satisfied. Hence, only the phase of the square wave decides the following motion of the solution. In this case, ϕ_3 must be larger than $2p_3\pi$. Because when x_3 hits the transitional condition $x_3=1$, $f_3(\tau)$ must be negative (see Eq. (29)). The Poincaré map T_3 can be derived as one-dimensional map as similar to the case of the circuit 1. Figure 13 shows an example of T_3. The form of T_3 is similar to T_1 and chaotic and quāsi-periodic attractors observed from the circuit 3 are well explained by the sine-circle map. The 1-parameter bifurcation diagram of T_3 is shown in Fig. 14.

Lastly, consider the case that the TVR varies

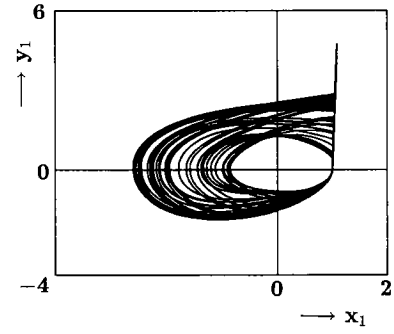

Fig. 16 Chaotic attractor obtained from the model with the TVR varying sinusoidally.
(a_s=0.48, b_s=0.245, ω_s=1.4, ε_s=0.02)

sinusoidally as shown in Fig. 15. Figure 16 shows an example of the chaotic attractors observed from the circuit 1. The parameters a_s, b_s are selected as the area contained by the sine wave and τ-axis is the same as the area contained by the square wave and τ-axis. We can confirm that similar attractors can be observed for some parameter values.

6. Conclusions

In this paper, we have analyzed four simple circuits with time-varying resistors. By using a degeneration technique we derived the one-dimensional Poincaré maps and confirmed that three circuits model generate various chaotic phenomena. Moreover, we carried out circuit experiments and confirmed the validity of the analyzing results.

Our future research is to calculate the Lyapunov exponents and to investigate the detailed bifurcation phenomena.

Acknowledgment

The authors would like to thank Assoc. Prof. Toshimichi Saito of Hosei University and Assist. Prof. Naohiko Inaba of Utsunomiya University for their valuable discussions.

References

(1) Chua, L. O., Komuro, M. and Matsumoto, T., "The Double Scroll Family," *IEEE Trans. Circuits Syst.*, vol. CAS-33, no. 11, pp. 1072-1118, 1986.
(2) Endo, T. and Chua, L. O., "Bifurcation Diagrams and Fractal Basin Boundaries of Phase-Locked Loop Circuits," *IEEE Trans. Circuits Syst.*, vol. CAS-37, no. 4, pp. 534-540, 1990.
(3) Inoue, M., "A Method of Analysis for the Bifurcation of the Almost Periodic Oscillation and the Generation of Chaos in a Parametric Excitation Circuit," *Trans. IEICE Japan*, vol. J68-A, no. 7, pp. 621-626, Jul. 1985.
(4) Tomiyasu, R., Kitagawa, T. and Itoh, M., "Chaotic Solutions in the Duffing-Mathieu's Equation," *Trans. IEICE Japan*, vol. J71-A, no. 6, pp. 1337-1338, Jun.

1988.
(5) Inaba, N., Saito, T. and Mori, S., "Chaotic Phenomena in a Circuit with a Negative Resistance and an Ideal Switch of Diodes," *Trans. IEICE*, vol. E70, no. 8, pp. 744-754, 1987.
(6) Saito, T., "On a Chaotic Family Including One Diode," *Trans. IEICE Japan*, vol. J71-A, no. 6, pp. 1275-1281, 1988.
(7) Inaba, N. and Mori, S., "Chaos via Torus Breakdown in a Piecewise-Linear Forced van der Pol Oscillator with a Diode," *IEEE Trans. Circuits Syst.*, vol. CAS-38, no. 4, pp. 398-409, 1991.
(8) Outlund, S., Rand, D., Sethana, J. and Siggia, E., "Universal Properties of Transition from Quasi-Periodicity to Chaos in Dissipative Systems," *Physica 8D*, pp. 303-342, 1983.
(9) Kaneko, K., "Supercritical Behavior of Disordered Orbits of a Circle Map," *Prog. Theor. Phys.*, vol. 72, pp. 1089-1103, 1984.

Appendix: Proof of Eq. (34)-(36)

At first, define the following functions of ε_i. Note that the time function $f_i(\tau)$ can be regarded as a constant, because $f_i(\tau)$ takes only two constant values.

$$\zeta_{i\pm}(\varepsilon_i)=-\{\varepsilon_i f_i(\tau)+1\} \pm\sqrt{\{\varepsilon_i f_i(\tau)+1\}^2-4\varepsilon_i\{\varepsilon_i+f_i(\tau)\}} \quad (i=1, 3)$$

$$\eta_{2\pm}(\varepsilon_2)=-\{\varepsilon_2 f_2(\tau)+1\}\pm\sqrt{\{\varepsilon_2 f_2(\tau)+1\}^2-4\varepsilon_2^2} \qquad (A\cdot1)$$

These functions correspond to the numerator of Eq. (25).

$\zeta_{i\pm}(\varepsilon_i)$ and $\eta_{2\pm}(\varepsilon_2)$ can be expanded to Maclaurin series and are approximated by its lower terms as

$$\zeta_{i+}(\varepsilon_i)=-2\varepsilon_i f_i(\tau)-2\varepsilon_i^2-2\varepsilon_i^3 f_i(\tau)+O(\varepsilon_i^4) \quad (i=1, 3)$$

$$\zeta_{i-}(\varepsilon_i)=-2+2\varepsilon_i^2+2\varepsilon_i^3 f_i(\tau)+O(\varepsilon_i^4) \quad (i=1, 3)$$

$$\eta_{2+}(\varepsilon_2)=-2\varepsilon_2^2+2\varepsilon_2^3 f_2(\tau)+O(\varepsilon_2^4)$$

$$\eta_{2-}(\varepsilon_2)=-2-2\varepsilon_2 f_2(\tau)+2\varepsilon_2^2-2\varepsilon_2^3 f_2(\tau)+O(\varepsilon_2^4) \qquad (A\cdot2)$$

By substituting (A·2) to (25), $\lambda_{i\pm}(\tau)$ is represented as follows.

$$\lambda_{i+}(\tau)=-f_i(\tau)-\varepsilon_i-\varepsilon_i^2 f_i(\tau)+O(\varepsilon_i^3) \quad (i=1, 3)$$

$$\lambda_{i-}(\tau)=-\frac{1}{\varepsilon_i}+\varepsilon_i+\varepsilon_i^2 f_i(\tau)+O(\varepsilon_i^3) \quad (i=1, 3)$$

$$\lambda_{2+}(\tau)=-\varepsilon_2+\varepsilon_2^2 f_2(\tau)+O(\varepsilon_2^3)$$

$$\lambda_{2-}(\tau)=-\frac{1}{\varepsilon_2}-f_2(\tau)+\varepsilon_2-\varepsilon_2^2 f_2(\tau)+O(\varepsilon_2^3) \qquad (A\cdot3)$$

From Eq. (A·3), Eq. (34) is proved.

The eigenspaces $E_{i+}(\tau)$ $(i=1, 2, 3)$ are represented as follows.

$$E_{1+}(\tau):\ x_1-\frac{f_1(\tau)}{f_1(\tau)+\varepsilon_1}+\{\lambda_{1+}(\tau)+f_1(\tau)\}\left\{y_1+\frac{1}{f_1(\tau)+\varepsilon_1}\right\}=0$$

$$E_{2+}(\tau):\ x_2-\lambda_{2+}(\tau)\left(y_2-\frac{1}{\varepsilon_2}\right)=0$$

$$E_{3+}(\tau):\ \{\lambda_{3+}(\tau)+f_3(\tau)\}x_3+y_3=0 \qquad (A\cdot4)$$

By substituting (A·3) into (A·4), (35) is proved easily.

At last, Eq. (36) can be proved by using Eqs. (A·3) and (A·4).

Yoshifumi Nishio was born in Mie, Japan, on January 24, 1966. He received the B.E. and M.E. degrees in Electrical Engineering from Keio University, Yokohama, Japan, in 1988 and 1990, respectively. He is currently working towards the Ph. D. degree in the Department of Electrical Engineering, Keio University. His research interests are in nonlinear circuits, network theory and cryptosystem. He is a student member of IEEE.

Shinsaku Mori was born in Kagoshima, Japan, on August 19, 1932. He received the B.E., M.E. and Ph. D. degrees in Electrical Engineering from Keio University, Yokohama, Japan, in 1957, 1959 and 1965, respectively. He is presently a Professor of Department of Electrical Engineering, Keio University. His research interests are in nonlinear circuit and communication engineering.